V European Conference on Computational Fluid Dynamics
ECCOMAS CFD 2010
J. C. F. Pereira and A. Sequeira (Eds)
Lisbon, Portugal,14-17 June 2010

NUMERICAL MODELING OF FLOW DYNAMICS INDUCED BY FRUIT FLIES DURING FREE-FLIGHT

Andrei Shishkin* **and Claus Wagner†**

German Aerospace Center (DLR), Institute for Aerodynamics and Flow Technology,
Bunsenstr. 10, D-37073, Göttingen, Germany
e-mail: *Andrei.Shishkin@dlr.de, †Claus.Wagner@dlr.de

Key words: free flight maneuvers, direct numerical simulation, moving mesh, OpenFoam

Abstract. *Numerical investigations of the insect free-flight aerodynamics are performed by means of three-dimensional Direct Numerical Simulations (DNS) of the flow around a fruit fly during free-flight maneuvers using the OpenFOAM toolkit. The governing equations are the incompressible Navier-Stokes equations in arbitrary Lagrangian-Eulerian formulation (ALE). The model of a fruit fly is constructed as a set of movable solid parts that combined with the geometry of the computational domain provides up to 12 degrees of freedom. In order to avoid inappropriately high mesh deformation, the moving mesh is realized as a sequence of slightly deforming meshes together with an interpolation of predicted flow fields during the mesh transition. The used data fruit fly kinematics are prescribed as obfained from detailed experimental studies of Drosophila free-flight maneuvers. Using the developed adapted OpenFoam toolkit a first test simulation of a 1-degree-of-freedom wing motion with a full stroke of* 160° *of a fixed fruit-fly is performed. The obtained flow fields reveal highly unsteady and vortical flow fields around the wings. The shedding of leading edge vortices, which play an important role for the insect aerodynamics, and the distribution of the pressure fields and the surface forces are also studied and will be presented at the conference.*

1 INTRODUCTION

The study of the insect flight performance reveals the sophisticated mechanism of generation of aerodynamic forces, which can be considered as an interactive combination of delayed stall, rotational circulation, and wake capture.[1] Many theoretical aspects are studied numerically in simplified 2D simulations[2] as well as in full 3D unsteady simulations,[3] which is computationally more difficult. Considering mesh based numerical methods (e.g. finite volume method) the problems induced by the insects motion are the most challenging. The insects locomotion during some free-flight maneuvers are characterized by complicated folded wings stroke with high amplitudes including clapping of the wings at the end of upstroke. The implementation of the wings motion with methods making use of the framework of Arbitrary Lagrangian-Eulerian (ALE)[4] can lead to an inadmissible mesh deformation. Additionally, in the case of non-hovering flight at least translational and rotational movement of an insect model or the complete computational domain also have be accounted for.

In this work we consider a two-step approach for numerical modeling of free-flight fruit fly maneuvers. The fruit fly motion is examined in two different phases. First, the computational domain moves as a solid body together with the fruit-fly body. This motion is accounted for mathematically by adding a term to the incompressible Navier-Stokes equations. Second, the simulation of the wings strokes is performed in a fixed domain using the ALE method.

In the next Section we describe shortly the geometrical insect model derived from the data obtained by P.Schützner and O.-F.Lehmann[5] in their experimental study of free-flight maneuver of a fruit fly (*Drosophila*). Section 3 contains the detailed description of the developed approach including an orthogonal transformation of the computational domain and related changes to the Navier-Stokes equations. In Section 4 results of test simulations of a simplified 1-degree-of-freedom fruit fly motion are presented.

2 EXPERIMENTAL DATA AND GEOMETRICAL MODEL

In P.Schützner and O.-F.Lehmann[5] the experimentally obtained free-flight kinematics are presented as time series of coordinates of fixed points at the body and the wings of a fruit fly during free-flight maneuver. The visualization of the marker paths is depicted on Fig. 1. Here complicated folded lines are produced by the points located at the tips and the trailing edge of the wings. The slightly disturbed lines correspond to points connected with the body.

The fruit fly model is constructed geometrically as a combination of three solid parts: the first one is the body, i.e. head-thorax-abdomen system, and the two others are the wings. One more accepted constraint is that the wing base points are attached to the fruit fly body. In this case the number of degrees of freedom (DoF) equals to 12: six degrees of freedom represent the fruit fly body motion and the wings rotation is described with additional 6 DoF.

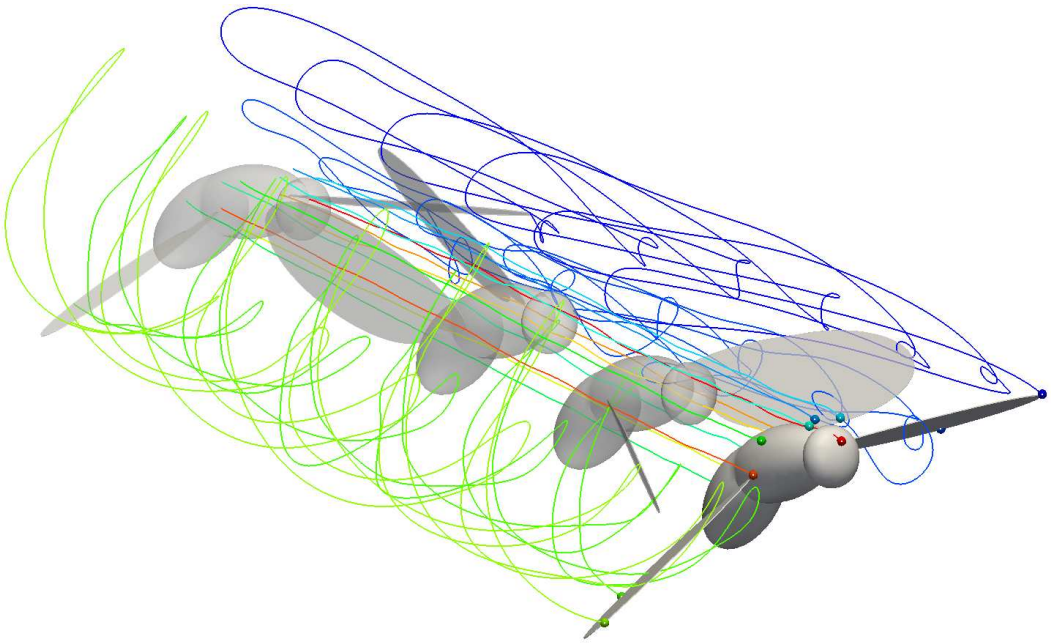

Figure 1: Visualization of the experimentally obtained free-flight kinematics of a fruit fly using trajectories of some points on the fruit fly.

In order to investigate the problem we introduce a two-step approach. First, we define the moving orthogonal coordinate system attached to the flies body. Then we consider the deformations invoked by the wings rotation. The first step demands for certain changes to Navier-Stokes equations, and the second one is realized using the standard Arbitrary Lagrangian-Eulerian (ALE) approach.[4]

3 THE TRANSFORMATION OF COORDINATE SYSTEM AND THE GOVERNING EQUATIONS

The body attached coordinate system can be constructed based on a set of three points (not lying on a straight line) which are regarded to be immovable relative to the body. One of them can be considered as the origin of the new coordinate system, and the whole set of three points is used to construct basis vectors rigidly bound with the points, and hence, with the body.

For the considered case we take the point of the center of gravity (CoG) and two wing base points. Fig.2 illustrates the chosen point set. The blue point is the CoG point which is considered as the origin of the moving coordinate system, the red points are the wings base points. The time varying coordinates of the CoG in the global coordinate system are denoted by $\mathbf{s}(t)$. The basis vectors $\mathbf{e}_i(t)$, $i = 1, 2, 3$ are constructed as follows. The vector $\mathbf{e}_1(t)$ is obtained by normalization of the vector pointing from CoG to the middle point of the wing base interval. The unit vector $\mathbf{e}_3(t)$ is orthogonal to the plane defined by the point set. And finally, $\mathbf{e}_2(t)$ is the vector product of $\mathbf{e}_3(t)$ and $\mathbf{e}_1(t)$. Thus,

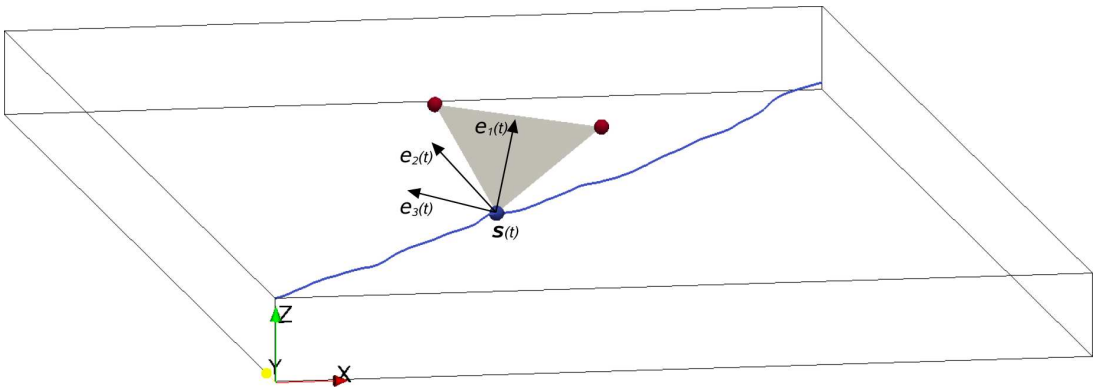

Figure 2: The path of the point of center of gravity (blue) of the fruit fly and the wing base points (red).

$\{\mathbf{e}_i(t); i = 1, 2, 3\}$ are orthonormal vectors, i.e. $(\mathbf{e}_i(t), \mathbf{e}_j(t)) = \sigma_{i,j}$, $i, j = 1, 2, 3$.

Consider the matrix $\mathcal{E}(t) = (\mathbf{e}_1(t), \mathbf{e}_2(t), \mathbf{e}_3(t))$ comprised by the vectors $\{\mathbf{e}_i(t); i = 1, 2, 3\}$ and the matrix

$$\mathcal{O}(t) = \mathcal{E}(t)\mathcal{E}(t_0)^T, \tag{1}$$

where t_0 denotes the initial time, and $()^T$ symbolizes a transposed matrix. One can see that due to orthogonality of the unit vectors $\mathbf{e}_i(t)$, $i = 1, 2, 3$ the matrix $\mathcal{E}(t)$ is an orthogonal matrix. The matrix $\mathcal{O}(t)$ is also orthogonal as a product of two orthogonal matrices, i.e.

$$\mathcal{O}\mathcal{O}^T = \mathbf{I}, \tag{2}$$

where $\mathbf{I} = (\sigma_{i,j})$ is the identity matrix. The transformation $\mathbf{x} \to \tilde{\mathbf{x}}(t)$ defined as

$$\tilde{\mathbf{x}} = \mathcal{O}(\mathbf{x} - \mathbf{s}) \tag{3}$$

leads to the coordinates $\tilde{\mathbf{x}}$ in the coordinate system attached to the moving body. The inverse transformation reads

$$\mathbf{x} = \mathcal{O}^T\tilde{\mathbf{x}} + \mathbf{s}. \tag{4}$$

Next, the incompressible dimensionless Navier-Stokes equations read

$$\frac{d\mathbf{u}}{dt} = \frac{1}{Re}\nabla^2\mathbf{u} - \nabla p + \mathbf{f}, \quad \nabla \cdot \mathbf{u} = 0 \tag{5}$$

where

$$\frac{d}{dt} = \frac{\partial}{\partial t} + (\mathbf{u} \cdot \nabla) \tag{6}$$

is a total time derivative, Re is the Reynolds number, p and $\mathbf{u}$ are the pressure and the velocity fields, respectively, and $\mathbf{f}$ is a driving force (we suppose here that $\mathbf{f} = 0$).

We apply the transformation (3) to Eqs. (5) to obtain adapted Navier-Stokes equations involving the velocity field $\tilde{\mathbf{u}} = \partial\tilde{\mathbf{x}}(t)/\partial t$.

Differentiating Eq.(4) with respect to t leads to

$$\mathbf{u} = \mathcal{O}^T \frac{\partial \tilde{\mathbf{x}}}{\partial t} + \frac{\partial \mathcal{O}^T}{\partial t}\tilde{\mathbf{x}} + \frac{\partial \mathbf{s}}{\partial t} = \mathcal{O}^T \tilde{\mathbf{u}} + \frac{\partial \mathcal{O}^T}{\partial t}\tilde{\mathbf{x}} + \frac{\partial \mathbf{s}}{\partial t} \tag{7}$$

where $\tilde{\mathbf{u}}$ is the velocity field in the moving coordinate system.

Using (3), we find the operator $\nabla = (\partial/\partial x_1, \partial/\partial x_2, \partial/\partial x_3)^T$ and the Laplacian ∇^2 in the moving coordinates $\tilde{\mathbf{x}}$

$$\nabla = \mathcal{O}^T \tilde{\nabla}, \quad \nabla^2 = \tilde{\nabla}^2, \tag{8}$$

where $\tilde{\nabla} = (\partial/\partial \tilde{x}_1, \partial/\partial \tilde{x}_2, \partial/\partial \tilde{x}_3)^T$.

The substitution of the relation (7) into momentum equation (5) accounting that

$$\nabla^2 \left(\frac{\partial \mathcal{O}^T}{\partial t}\tilde{\mathbf{x}} + \frac{\partial \mathbf{s}}{\partial t} \right) = 0$$

yields

$$\mathcal{O}^T \frac{d\tilde{\mathbf{u}}}{dt} + \frac{\partial \mathcal{O}^T}{\partial t}\tilde{\mathbf{u}} + \frac{d}{dt}\left(\frac{\partial \mathcal{O}^T}{\partial t}\tilde{\mathbf{x}} + \frac{\partial \mathbf{s}}{\partial t} \right) = \mathcal{O}^T \left(\frac{1}{Re}\tilde{\nabla}^2 \tilde{\mathbf{u}} - \tilde{\nabla} p \right). \tag{9}$$

or,equivalently,

$$\frac{d\tilde{\mathbf{u}}}{dt} = \frac{1}{Re}\tilde{\nabla}^2 \tilde{\mathbf{u}} - \tilde{\nabla} p - \mathcal{O}\frac{d}{dt}\left(\frac{\partial \mathcal{O}^T}{\partial t}\tilde{\mathbf{x}} + \frac{\partial \mathbf{s}}{\partial t} \right) - \mathcal{O}\frac{\partial \mathcal{O}^T}{\partial t}\tilde{\mathbf{u}}. \tag{10}$$

Note that the obtained Eq.(10) differs from the momentum equation (5) only with an additional drive force term $\mathbf{f}(\mathbf{u}, \mathbf{x}, t)$.

For the continuity equation in (5) using Eq.(7) and the matrix orthogonality property (2) we have the following

$$\begin{aligned} \nabla \cdot \mathbf{u} &= \mathcal{O}^T \tilde{\nabla} \cdot (\mathcal{O}^T \tilde{\mathbf{u}}) + \mathcal{O}^T \tilde{\nabla} \cdot \left(\frac{\partial \mathcal{O}^T}{\partial t}\tilde{\mathbf{x}} + \frac{\partial \mathbf{s}}{\partial t} \right) \\ &= \tilde{\nabla} \cdot (\mathcal{O}\mathcal{O}^T \tilde{\mathbf{u}}) + \tilde{\nabla} \cdot \left(\mathcal{O}\frac{\partial \mathcal{O}^T}{\partial t}\tilde{\mathbf{x}} + \mathcal{O}\frac{\partial \mathbf{s}}{\partial t} \right) \\ &= \tilde{\nabla} \cdot \tilde{\mathbf{u}} + \tilde{\nabla} \cdot \left(\mathcal{O}\frac{\partial \mathcal{O}^T}{\partial t}\tilde{\mathbf{x}} \right) = 0. \end{aligned} \tag{11}$$

Further, taking the time derivative in Eq.(2) we obtain

$$\frac{\partial}{\partial t}\left(\mathcal{O}\mathcal{O}^T \right) = \mathcal{O}\frac{\partial \mathcal{O}^T}{\partial t} + \frac{\partial \mathcal{O}}{\partial t}\mathcal{O}^T = \mathcal{O}\frac{\partial \mathcal{O}^T}{\partial t} + \left(\mathcal{O}\frac{\partial \mathcal{O}^T}{\partial t} \right)^T = \mathbf{0}. \tag{12}$$

It means that the matrix $\mathcal{O}\partial\mathcal{O}^T/\partial t$ is skew-symmetric, and hence, all the diagonal elements are equal to zero. Thus,

$$\tilde{\nabla}\cdot\left(\mathcal{O}\frac{\partial\mathcal{O}^T}{\partial t}\tilde{\mathbf{x}}\right)=\mathrm{tr}\left(\mathcal{O}\frac{\partial\mathcal{O}^T}{\partial t}\right)=0.$$

The substitution of the last equation into the Eq.(11) together with Eq.(10) implies

$$\frac{\partial\tilde{\mathbf{u}}}{\partial t}+(\tilde{\mathbf{u}}\cdot\tilde{\nabla})\tilde{\mathbf{u}}=\frac{1}{Re}\tilde{\nabla}^2\tilde{\mathbf{u}}-\tilde{\nabla}\tilde{p}+\tilde{\mathbf{f}},\quad\tilde{\nabla}\cdot\tilde{\mathbf{u}}=0, \tag{13}$$

where

$$\tilde{\mathbf{f}}=-2\mathcal{O}\frac{\partial\mathcal{O}^T}{\partial t}\tilde{\mathbf{u}}-\frac{\partial}{\partial t}\left(\mathcal{O}\frac{\partial\mathcal{O}^T}{\partial t}\right)\tilde{\mathbf{x}}-\frac{\partial^2\mathbf{s}}{\partial t^2} \tag{14}$$

And finally, following the standard ALE approach for a moving (deforming) mesh we obtain the following equations

$$\frac{\partial\tilde{\mathbf{u}}}{\partial t}+((\tilde{\mathbf{u}}-\mathbf{u}_{mesh})\cdot\nabla)\tilde{\mathbf{u}}=\frac{1}{Re}\nabla^2\tilde{\mathbf{u}}-\nabla\tilde{p}+\tilde{\mathbf{f}},\quad\nabla\cdot\tilde{\mathbf{u}}=0, \tag{15}$$

where $\mathbf{u}_{mesh}$ is the velocity of the mesh deformation, the intermediate velocity $\tilde{\mathbf{u}}$ is linked to the velocity $\mathbf{u}$ by Eq.(7) and $\tilde{\mathbf{f}}$ is defined by Eq.(14). Note that the boundary conditions for the velocity field are corrected taking into account Eq.(7).

The above described approach has been implemented using the OpenFOAM toolkit.

4 RESULTS OBTAINED FOR SIMPLIFIED FRUIT FLY MOTION

In this section we present some results obtained in Direct Numerical Simulations (DNS) of a flow induced by a simplified fruit fly model which we defined in order to test the implemented algorithms.

4.1 Computational setup

The geometry of a fruit fly model and the computational domain are depicted on Fig.3. The characteristic size of the fruit fly model is about $2.5mm$. The spherical computational domain has a diameter of $30mm$.

The considered fruit fly motion is defined by the motionless body and an 1-DoF rotation of the wings. The angle of the wing rotation is described by the sinusoidal law with the stroke swing of 160° and the frequency of $200sec^{-1}$. In this case the equations Eq.(15) are reduced to the incompressible dimensionless Navier-Stokes equations in ALE formulation

$$\frac{\partial\mathbf{u}}{\partial t}+((\mathbf{u}-\mathbf{u}_{mesh})\cdot\nabla)\mathbf{u}=\frac{1}{Re}\nabla^2\mathbf{u}-\nabla p,\quad\nabla\cdot\mathbf{u}=0, \tag{16}$$

where $Re=100$.

The boundary conditions are:

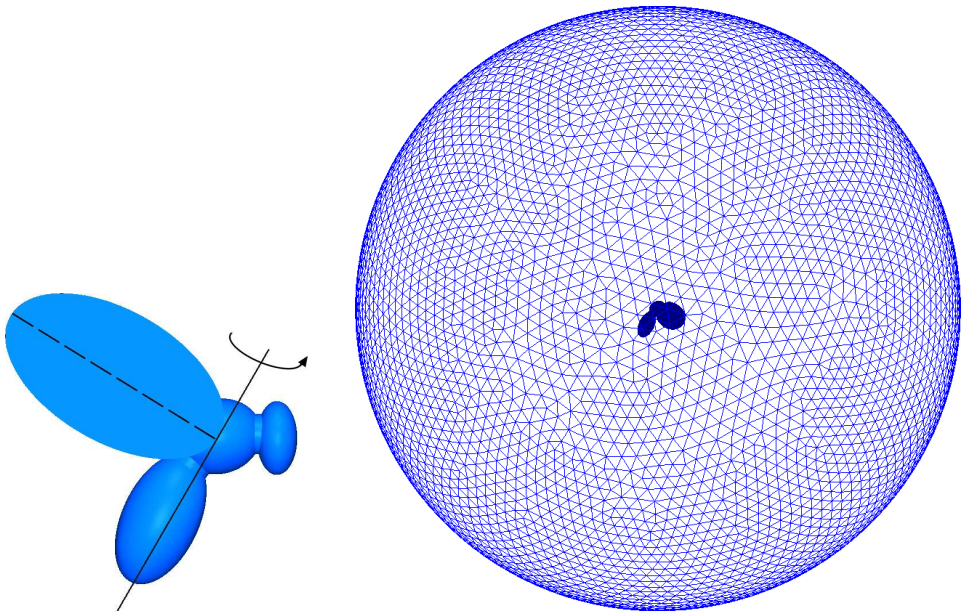

Figure 3: The geometrical model of fruit fly with one degree of freedom (left) and the computational domain(right)

- at the exterior (spherical) boundary – zero gradient for the velocity field and fixed zero value for the pressure;
- at the motionless surface of the body – wall boundary conditions for the velocity field ($\mathbf{u} = 0$) and zero gradient for the pressure;
- at the moving surface of the wings – moving wall boundary conditions for the velocity field ($\mathbf{u} \approx \mathbf{u}_{mesh}$) and zero gradient for the pressure;

In order to realize the wings motion some special OpenFOAM libraries are implemented. The mesh motion velocity $\mathbf{u}_{mesh}$ is calculated using Laplacian mesh motion solver with *inverse quadratic* diffusivity. Due to the high amplitude of the wing stroke the mesh motion produces some inadmissibly deformed cells. To avoid this effect, a set of four meshes is used. Each mesh of the set is constructed for a certain range of rotation angle and provides there high quality cells. The meshes are changed together with the interpolation of flow fields.

4.2 Predicted flow fields

The objectives for these simulations are twofold. First we wanted to test the developed computational routines, mesh generation/deformation procedures and other numerical problems, and second obtain first results of the flapping wing aerodynamics. Special attention is paid to the spatial distribution of the pressure, the surface distribution of the forces acting on the wings and the body, vortex formation and the vorticity field.

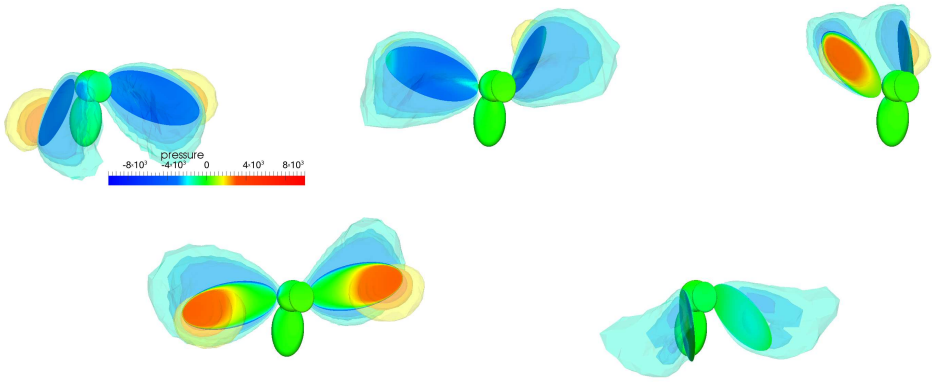

Figure 4: Isosurfaces of the dynamic pressure obtained in DNS at the different wing positions. The fruit fly surface is coloured with the pressure values.

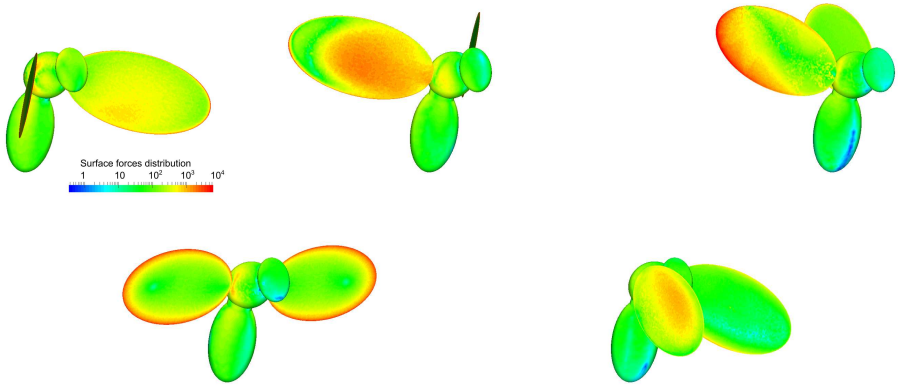

Figure 5: The distribution of the magnitude of the forces acting on the surface obtained in DNS at the different phase of the wings stroke

Some results obtained in these DNS are depicted on Fig.4–7.

The aerodynamic forces acting on a fruit fly are the result of the integration of the normal component of the local stress $\sigma = -p\mathbf{I} + \tau$ over the complete surface. So, it is important to get the information of the distribution of both pressure and viscous force components. In Fig.4 the surface distribution of the pressure and some pressure isosurfaces for the different times and in Fig.5 the distribution of the surface forces magnitude $|\sigma\mathbf{n}|$ are presented. Comparing the distributions of the pressure and the surface forces one concludes that local extrema as well as extremal points are different at a different wing positions. The contribution of pressure and viscous components strongly dependent on the wings position. Nevertheless, it is observed that the largest values of the surface forces develop at the edges of the wings.

The distribution of the vorticity magnitude shown in Fig.6 also reveals the dependence on the stroke phases. The highest values are observed close to the wings edges as a

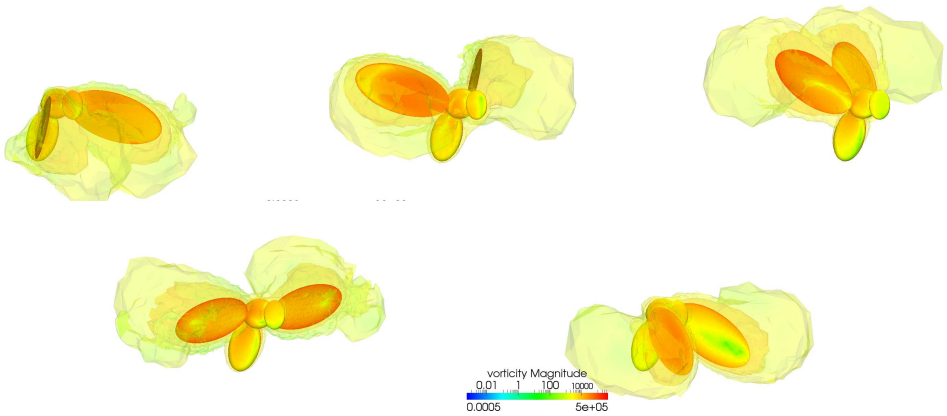

Figure 6: Isosurfaces of vorticity magnitude at the different wing positions.

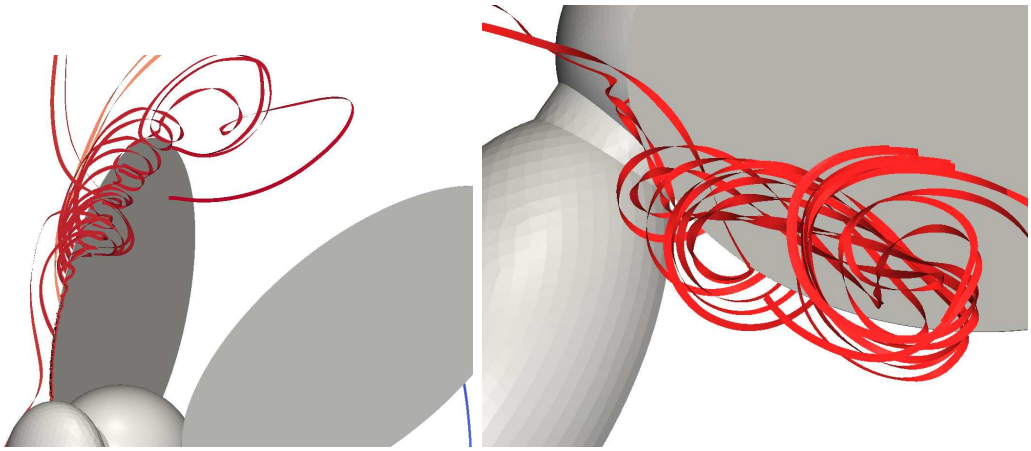

Figure 7: Streamlines of the flow around leading (left) and trailing (right) edges

result of high shear gradients. The vortices at the leading and trailing edge (see Fig.7) dynamically appear and disappear in accordance with the generation of lift and drag.

5 CONCLUSIONS

In the work we present the algorithms and the methodology to perform DNS of the flow around fruit fly during free-flight maneuver using experimentally obtained kinematics. The developed approach is based on the superposition of orthogonal transformation of the computational domain and mesh deformation in the ALE framework.

Using the algorithms together with the generation of a few new meshes DNS of a simplified 1-DoF fruit fly motion with a full stroke of 160° is realized. The analysis of the obtained results shows that the flow simulation of a stroke with the wings rotating in one direction leads to reasonable aerodynamics including the generation of leading and trailing edge vortices.

REFERENCES

[1] M. Dickinson, F.-O. Lehmann and S. Sane, Wing Rotation and the Aerodynamic Basis of Insect Flight, *Science* **284**, 1954–1960 (1999)

[2] F.M. Bos, D.Lentink, B.W. Oudheusden and H. Bijl, Influence of wing kinematics on aerodynamic performance in hovering insect flight, *J. Fluid Mech.* **594**, 341–368 (2008)

[3] R. Ramamurti and W.C. Sandberg, A computational investigation of the three-dimensional unsteady aerodynamics of Drosophila hovering and maneuvering, *Journal of Experimental Biology* **210**, 881–896 (2007)

[4] J.Ferziger and M.Peric, Computational Methods for Fluid Dynamics, *Springer-Verlag Berlin*, 3rd ed., (2002)

[5] P. Schützner and F.-O. Lehmann, High-speed analysis of wing and body motions in flying Drosophila using fluorescent markers, *FIR meeting*, Ascona, Switzerland, 103–104 (2007).